EFDA–JET–CP(08)05/12

M. Maslov, H. Weisen, C. Angioni and JET EFDA contributors

Density Profile Behavior in JET H-mode Plasmas

“This document is intended for publication in the open literature. It is made available on the understanding that it may not be further circulated and extracts or references may not be published prior to publication of the original when applicable, or without the consent of the Publications Officer, EFDA, Culham Science Centre, Abingdon, Oxon, OX14 3DB, UK.”

“Enquiries about Copyright and reproduction should be addressed to the Publications Officer, EFDA, Culham Science Centre, Abingdon, Oxon, OX14 3DB, UK.”

Density Profile Behavior in JET H-mode Plasmas

M. Maslov[1], H. Weisen[1], C. Angioni[2] and JET EFDA contributors*

JET-EFDA, Culham Science Centre, OX14 3DB, Abingdon, UK

[1]EPFL, CRPP-AE, CH-1015 Lausanne, Switzerland
[2]Max-Planck-Institut für Plasmaphysic, EUROATOM Association, D-85748 Garching
** See annex of F. Romanelli et al, "Overview of JET Results",*
(Proc. 22[nd] IAEA Fusion Energy Conference, Geneva, Switzerland (2008)).

Preprint of Paper to be submitted for publication in Proceedings of the
22nd IAEA Fusion Energy Conference, Geneva, Switzerland.
(13th October 2008 - 18th October 2008)

ABSTRACT.
The degree of peaking of the density profile has profound implications for reactor operation. As an independent complement to previous studies, density peaking in the JET tokamak was investigated on the most recent dataset, comprising virtually all experiments performed in 2006 and 2007. Unlike previous studies, this work focuses on low collisionality data as most representative of reactor conditions. The study confirms that collisionality is the most important parameter governing density peaking in H-mode, followed by the NBI particle flux and/or the T_i/T_e temperature ratio. For the first time in JET a modest, albeit significant dependence of peaking on internal inductance, or magnetic shear is seen. The experimental behavior is compared to an extensive database of simulations based on linear gyrokinetic calculations using the GS2 code. The predictions from GS2 simulataions based on the highest linear growth rate modes are in good agreement with experimental observations. They are also corroborated by initial results from the non-linear code GYRO.

1. INTRODUCTION.

This work continues the study previously undertaken on AUG and JET [1,2,3], which has shown that collisionality is the most important scaling parameter for density peaking in Hmodes. It uses an entirely new experimental dataset, obtained from experiments performed in 2006 and 2007. The aim of this study is to revisit all parameter dependencies on an independent database, with emphasis on low collisonalities and to provide a comparison with predictions from quasi-linear and non-linear gyrokinetic theory.

The effective collisionality definition used in this work is: $\nu_{eff} = 2\times10^{-14} R\langle n_e\rangle/\langle T_e\rangle^2$
As a measure of density peaking we use the ratio of average density inside r/a=0.2 surface and overall volume average density, $n_{0.2}/\langle n_e\rangle$. We also use the normalized density gradient R/L_n at r/a = 0.5. Minor radius is defined as a flux surface half width at the equatorial plane, and the gradient was calculated by a linear fit over r/a = 0.2-0.8.

The dimensionless particle source is defined as $\Gamma' = eT_iS/Q_i$, where S ($1/m^2/s$) is the particle flux and Qi (eV/m2/s) is the ion heat flux through a given flux surface (here always taken at r/a = 0.5), e is the electron charge and T_i is the local ion temperature.

2. EXPERIMENTS.

For the analysis of experimental data we have chosen ~270 plasma discharges. All samples are from H-modes with stationary phases longer than 1 second. All of the discharges in this dataset are dominantly NBI heated. About 20% of the discharges also had some LHCD heating and 50% of them had additional ICRH heating, which allowed us to obtain a variation of l_i and T_i/T_e parameters. Density profile was measured by two independent diagnostics: LIDAR Thomson scattering and inversion of Far Infrared Interferometer line integrated density (6 chords covering the whole plasma section). They provided consistent results for both the peaking factor and the density gradient measurements. NBI power and particle deposition in the JET plasma core are calculated using the PENCIL code [6].

It was already shown in earlier JET experiments that density peaking in H-mode plasma scales with the logarithm of the effective collisionality [1-5]. The same tendency is clearly seen also in the recent JET plasmas studied in this paper (Fig.1) with an additional feature: around $\nu_{eff} \sim 0.5$ there appears to be an inflexion point where the collisionality dependence disappears. The reason of this behavior may lie in the limited diagnostics resolution for measuring the edge part (pedestal) of the density profile. We limit our analysis to the low collisionality branch ($\nu_{eff} < 0.5$), which represents the monotonic $\nu_{eff}^{0.5}$ dependence and belongs to the relevant domain for ITER extrapolations.

The purpose of this experimental database analysis is to find the empirical relation(s) between density peaking and other dimensionless plasma parameters. We focus on the following 10 variables: ν_{eff}, Γ', ρ^* (the normalized Larmor radius), T_i/T_e, q_{95} (safety factor at 95% of poloidal flux), β_N, R/L_{Te}, R/L_{Ti}, l_i (internal inductance obtained from magnetic measurements), and δ (triangularity at the last closed flux surface). They are well spread which allows us to study their respective bivariate correlations (Table 1).

In this work we will use the square root of effective collisionality instead of the logarithm. For the empirical analysis that substitution does not produce a significant difference, but it will be easier for the comparison with simulation results presented later in the paper.

As one can see, density peaking is strongly correlated with $\nu_{eff}^{0.5}$. The parameters Γ', T_i/T_e and δ show a moderate correlation, β_N and li have the lowest (barely visible) correlation with density gradients and the other parameters (q_{95}, ρ^*, R/L_{Te}, R/L_{Ti}) are not relevant at all, confirming conclusions from an earlier dataset on JET [2]. For multivariable regression analysis we will use the linear fit in the form: $Y = c + \mathrm{sum}((a_j \pm \sigma(a_j))*X_j)$, where Y is the regressed variable, X_j are the regression variables (those listed in the table above), aj are the regression coefficients and $\sigma(a_j)$ are the standard deviations of a_j and correspond to a 66% confidence interval.

The best empirical scalings obtained here for the peaking factor are:

$$
\begin{aligned}
n_{0.2}/\langle n_e \rangle &= 1.96 \pm 0.04 - (0.88 \pm 0.07)\, \nu_{eff}^{0.5} \\
n_{0.2}/\langle n_e \rangle &= 1.78 \pm 0.05 - (0.74 \pm 0.07)\, \nu_{eff}^{0.5} + (1.58 \pm 0.32)\, \Gamma' \quad (1) \\
n_{0.2}/\langle n_e \rangle &= 1.74 \pm 0.05 - (0.81 \pm 0.07)\, \nu_{eff}^{0.5} + (0.18 \pm 0.04)\, T_i/T_e \\
n_{0.2}/\langle n_e \rangle &= 1.43 \pm 0.10 - (0.63 \pm 0.07)\, \nu_{eff}^{0.5} + (1.92 \pm 0.32)\, \Gamma' + (0.34 \pm 0.09)\, l_i \\
n_{0.2}/\langle n_e \rangle &= 1.31 \pm 0.12 - (0.70 \pm 0.07)\, \nu_{eff}^{0.5} + (0.25 \pm 0.04)\, T_i/T_e + (0.39 \pm 0.09)\, l_i
\end{aligned}
\qquad (1)
$$

The best empirical scalings obtained for the normalized gradient are:

$$
\begin{aligned}
R/L_n &= 4.59 \pm 0.21 - (3.95 \pm 0.38)\, \nu_{eff}^{0.5} \\
R/L_n &= 3.33 \pm 0.27 - (2.99 \pm 0.38)\, \nu_{eff}^{0.5} + (10.6 \pm 1.7)\, \Gamma' \\
R/L_n &= 3.07 \pm 0.33 - (3.47 \pm 0.36)\, \nu_{eff}^{0.5} + (1.23 \pm 0.21)\, T_i/T_e \quad (2) \\
R/L_n &= 2.32 \pm 0.56 - (2.69 \pm 0.40)\, \nu_{eff}^{0.5} + (11.59 \pm 1.75)\, \Gamma' + (0.99 \pm 0.49)\, l_i \\
R/L_n &= 1.67 \pm 0.64 - (3.12 \pm 0.38)\, \nu_{eff}^{0.5} + (1.44 \pm 0.23)\, T_i/T_e + (1.28 \pm 0.51)\, l_i
\end{aligned}
\qquad (2)
$$

Parameters Γ' and T_i/T_e cannot be included into the same regression fit due to high degree of correlation between them (a coefficient of 0.93 in Table1). The reason is in the properties of electron and ion heating produced by thermalizing beam particles [7], which results in ion heating being proportional to electron temperature for a fixed input NBI power, $\Gamma' = eT_iS/Q_i \sim \text{const} \cdot ET_i/T_e$. Relations connecting those parameters in our database are:

$$\Gamma' = -(0.027 \pm 0.008) - (0.045 \pm 0.009)\, v_{eff}^{0.5} + (0.118 \pm 0.006)\, T_i/T_e$$

or (3)

$$T_i/T_e = (0.34 \pm 0.06) + (0.30 \pm 0.08)\, v_{eff}^{0.5} + (7.58 \pm 0.36)\, \Gamma'$$

Including one of the two parameters generally increases the quality of the fit. We conclude that at least one is important for the density peaking, but it's impossible to decorrelate them in this particular database since one would need discharges with dominant electron heating (or ion heating of other than NBI nature). For the experiments considered in this paper there are no such data.

Among three-parameter fits the best ones combine $\{v_{eff}^{0.5}; \Gamma'; l_i\}$ and $\{v_{eff}^{0.5}; T_i/T_e; l_i\}$. The internal inductance is statistically significant in all parameter combinations with a regression coefficient in the range ~0.3-0.4. In our dataset li does have a modest effect on density peaking.

To make an empirically based prediction for ITER density profile, we assume $\langle n_e \rangle = 10^{20} m^{-3}$, $\langle T_e \rangle = 8$keV, $R_{mag} = 6.2$m, $\Gamma' = 0$, $T_i/T_e = 1$, which corresponds to the inductive reference scenario [8]. That gives us v_{eff}(ITER) = 0.19 and $n_{0.2}/\langle n_e \rangle$(ITER) = 1.42 – 1.55, R/L_n(ITER) = 2.0 – 2.8, depending which of the derived scales is used. The prediction for the peaking factor is in agreement with the extrapolations done in previous publications [1-3]. The expectations for R/L_n values are a bit lower in this work, but the value used here is calculated over the large density profile range and can be slightly biased with respect to definitions used in other publications.

3. GS2 SIMULATIONS.

We have evaluated the role of microturbulence predicted by linear gyrokinetic theory using a large number (>1000) of linear gyrokinetic simulations produced with GS2 flux tube code [9, 10] in electrostatic regime with input parameters representative of the experimental parameters. All simulations were done for r/a = 0.5 with fixed $R/L_{Te} = 6.0$, $q = 1.5$, $\hat{s} = 0.45$, $\kappa = 1.45$, $\kappa' = 0.1$, $\delta = 0.12$, $\delta' = 0.06$. While keeping these values constant, we independently varied 4 other parameters: R/L_n, R/L_{Ti}, T_i/T_e and v_{eff}. Since the simulations are linear, perturbed quantities grow indefinitely without saturation. However the ratio of particle flux and ion heat flux generated (which we denote as Γ_{GS2}) remains constant since it depends only on the mode structure and not on its final amplitude. This dimensionless value (ion heat flux is normalized by ion temperature) is the result of each particular GS2 run.

Simulations were done for 10 values of $k_y = 0.1, 0.2, \ldots 1.0$ and the heat and particle fluxes generated were calculated for the mode with the highest linear growth rate (fastest mode number was varied between 0.3 and 0.6 for different plasma conditions). The real mode frequency in our

simulations was always positive, which allows us to identify them as ITG modes.

For the first group of simulations we used 13 values of ν_{eff} between 0.04 and 0.8, 4 values of T_i/T_e (0.75, 0.85, 1.0, 1.15), 5 values of R/L_n (1.0, 1.8, 2.3, 2.8, 3.2), 4 values of R/L_{Ti} (6.0, 7.0, 8.0, 9.0). To facilitate the data analysis, we will split these simulations into 4 groups, corresponding to different R/L_{Ti} values and considered them separately.

In each of those groups, Γ_{GS2} is presented as a table as a function of the other three parameters: ν_{eff}, T_i/T_e and R/L_n. (Fig.2). To facilitate our comparison with the experimental results, we introduce an approximation for Γ_{GS2}. After some trial and error steps we found that Γ_{GS2} scales fairly linearly with T_i/T_e, $(\nu_{eff})^{1/2}$, $(R/L_n)^{3/2}$ and $(\nu_{eff})^{1/2}(R/L_n)^{3/2}$:

$$\Gamma_{GS2} = -0.146 + (0.0305 - 0.0081\nu_{eff}^{1/2})(R/L_n)^{3/2}\, 0.1\nu_{eff}^{1/2} + 0.0524 T_i/T_e \qquad (4)$$

The blue lines on Fig.2 correspond to Γ_{GS2} obtained from this simple fit. From this formula we can extract R/L_n as a function of other parameters:

$$\Gamma_{GS2} = \left(\frac{0.146 + \Gamma_{GS2} - 0.0524\, T_i/T_e - 0.1\sqrt{\nu_{eff}}}{0.0305 - 0.0081\sqrt{\nu_{eff}}} \right)^{2/3} \qquad (5)$$

The RMS deviation between real and approximated R/Ln values is ~0.066 and the maximum deviation found is 0.23 (at $R/L_n \sim 1.0$).

Note that Γ_{GS2} and Γ' have the same definition, so we can substitute ì' values to formula (5) to make a direct comparison with the experiment.

In figure 3 the normalized density gradient values obtained via formula 5 using experimental Γ', ν_{eff} and T_i/T_e parameters are plotted in color on top of the real measured R/L_n (grey points). There is good quantitative agreement between experimental and simulation predicted values, which comprises the same kind of scaling with effective collisionality. To compare GS2 simulation results with the linear empirical scaling we must exclude Γ' or T_i/T_e from (5) using relations (3) which describes their experimental cross-dependence. After that we evaluate the linear coefficients by calculating the partial derivatives.

$$\frac{\partial(R/L_n)}{\partial(T_i/T_e)} = 1.43 \pm 0.26 \quad \frac{\partial(R/L_n)}{\partial(\Gamma')} = 13.1 \pm 2.4$$

$$\frac{\partial(R/L_n)}{\partial(\sqrt{\nu_{eff}})} = 3.15 \pm 0.57 \text{ for the fit with } T_i/T_e \text{ and } \nu_{eff}^{1/2} \ (\Gamma' \text{ excluded}).$$

$$\frac{\partial(R/L_n)}{\partial(\sqrt{\nu_{eff}})} = 2.51 \pm 0.45 \text{ for the fit with } \Gamma' \text{ and } \nu_{eff}^{1/2} \ (T_i/T_e \text{ excluded}).$$

Uncertainty interval corresponds to variations of $R/L_n = 1.0\text{-}3.0$. Comparing with the empirical scalings (2) one can see that the GS2 simulations show a parametric dependence very similar to the experimental one.

3.1. SIMULATION RESULTS FOR DIFFERENT R/LTI VALUES

In the above we considered only the simulations with $R/L_{Te} = R/L_{Ti} = 6.0$. To estimate the effect of different R/L_{Ti} values on the predicted density gradients we will construct the functions $R/L_n = f(\Gamma', T_i/T_e, \nu_{eff})$ by analogy with (5) for other R/L_{Ti} values (7.0, 8.0, 9.0) and compare their output for JET experimental Γ', T_i/T_e and Ω_{eff} parameters.

$$R/L_{Ti} = 7.0: R/L_n = \left(\frac{0.12 + \Gamma' - 0.0511\ T_i/T_e - 0.082\sqrt{\nu_{eff}}}{0.0247 - 0.0057\sqrt{\nu_{eff}}} \right)^{2/3} \text{RMS} = 0.046 \qquad (9)$$

$$R/L_{Ti} = 8.0: R/L_n = \left(\frac{0.101 + \Gamma' - 0.049\ T_i/T_e - 0.07\sqrt{\nu_{eff}}}{0.0208 - 0.0042\sqrt{\nu_{eff}}} \right)^{2/3} \text{RMS} = 0.045 \qquad (8)$$

$$R/L_{Ti} = 9.0: R/L_n = \left(\frac{0.087 + \Gamma' - 0.047\ T_i/T_e - 0.062\sqrt{\nu_{eff}}}{0.018 - 0.0032\sqrt{\nu_{eff}}} \right)^{2/3} \text{RMS} = 0.05 \qquad (9)$$

In figure 4 we plot expected R/L_n values for various ion temperature gradients (obtained with expressions 7-9) as a function of the values expected for $R/L_{Ti} = 6$, our base case. The difference is noticeable at higher density gradients where R/Ln increases with R/L_{Ti}. At intermediate gradient values more typical for JET, there is no difference between various R/L_{Ti} cases and at the lowest R/L_n a weak inverse tendency is observed. Cross-correlation coefficient between R/Ln values calculated by formulas (5), (7-9) using JET experimental parameters and corresponding R/LTi values 6.0 ± 9.0 gives a factor of 0.18 for the cases $\nu_{eff} < 0.5$. So from the GS2 simulations we do not expect any noticeable R/L_{Ti} dependence for considered JET plasma conditions. This is consistent with our observations.

3.2. SHEAR DEPENDENCE IN SIMULATIONS AND EXPERIMENT.

In the empirical scaling (3) we used the internal inductance as a characteristic of safety factor profile, since this value is the easiest to obtain. In the simulations only local values of magnetic shear] can be used, so we establish a relation between l_i and $s = dq/dr \cdot Er/q$ in our database to compare the GS2 results with the experiment: $\hat{s}\ (0.5) \approx -0.35 + 0.92\ l_i$. The q profile was taken from the equilibrium code EFIT. That is very basic estimation, but only this one is available on a routine basis.

To estimate the effect of s in the simulation results, a separate smaller set of GS2 runs was produced. Three parameters were varied: R/L_n (1.8, 2.3, 2.8, 3.2), ν_{eff} (9 values between 0.03 and 0.8) and $\hat{s}$ (0.0, 0.3, 0.6, 0.9). An example of the simulation results one can see on Fig.5. Higher shear always leads to lower particle fluxes needed to maintain given density gradient, so higher mid-radius shear and as a consequence higher l_i should lead to stronger peaking.

Linear regression of R/L_n versus other parameters in this simulations group gives us an estimation of s effect on density gradient:

$\frac{\partial(R/L_n)}{\partial(\hat{s})} \sim 1.0$, which transforms into $\frac{\partial(R/L_n)}{\partial(l_i)} \sim 0.90$ if we use the relation between $\hat{s}$ (0.5) and l_i obtained from the database. We conclude that the GS2 linear simulations and JET observations agree within the error bars on the shear dependence too.

3.3 EXTRAPOLATION OF THE SIMULATIONS RESULTS TO Γ' = 0, T_i/T_e = 1 PLASMAS.

No particle source and $T_i = T_e$ condition is especially interesting since these parameters are expected for ITER plasmas. Fixing $\Gamma' = 0$ and $T_i/T_e = 1$ values in formula (5) we can calculate the expected density gradient as a function of collisionality (Fig.6). For ITER collisionality, $\nu_{eff} \sim 0.19$, the expected value is $R/L_n(ITER) \sim 1.7$

That is slightly lower than the values evaluated from empirical scalings (2) which predict the gradient to be in the range 2-3, depending on which scaling expression is used.

We should however keep in mind that according to GS2, both Γ' and T_i/T_e play a role. An experimental extrapolation based on a database, where like in the present one, these two quantities are strongly correlated, is therefore likely to suffer from uncertainties.

4. COMPARISON WITH PREVIOUS SIMULATION RESULTS AND NON-LINEAR GYRO RUN.

Study of GS2 simulation results with respect to particle transport in tokamaks was already done in [11]. According to these results, the particle flux produced by ITG turbulence is directed outwards for all realistic collisionality values, which appeared to be in contradiction with experimental observations. The main difference between the two studies is the part of ky spectrum which was considered. In the previous work the focus was on linear modes with maximum $\gamma/k_\perp^2$. This quasilinear method was motivated by nonlinear simulations of ITG/TEM turbulence in the collisionless limit [12], which identified the peak of heat and particle transport to match the maximum of $\gamma/k_\perp^2$.

But the recently done GYRO simulations have shown that in a collisional case the actual nonlinear spectrum is more complex and cannot be represented by $\gamma/k_\perp^2$ curve. In figure 7 the result of a GYRO run is drawn. This was in electrostatic regime, local Miller equilibrium, box size $L_x = 82\rho^*$, $L_y = 148\rho^*$ with resolution $\Delta_x = 0.58\ \rho^*$, 64 toroidal modes between $k_\theta\rho^*(min) = 0.043$ and $k_\theta\rho^*(max) = 2.68$. Physical parameters: $R/L_{Ti} = R/L_{Te} = 6.12$, $T_i/T_e = 1$, $s = 1.12$, $q = 1.33$, $\kappa = 1.38$, $\delta = 0.03$, $Z_{eff} = 2$, ν_{ei} (GYRO) $= \nu_{ei}$ $(a/c_s) = 0.018$, which corresponds to $\nu_{eff} \sim 0.2$.

For these plasma parameters the total particle flux calculated by GYRO is about zero, which means the input density gradient R/Ln is stationary. This is in a fair agreement with the linear GS2 prediction based on the fastest growth rate mode (Fig.6). The difference between two quasilinear approaches can be easily understood from the particle flux spectrum (Fig.7, bottom-right). Low k_y modes produce outward flux, while shorter wavelengths correspond to the inward part. So focusing linear analysis on the maximum of $\gamma/k_\perp^2$ ($k_y \sim 0.1$-0.2) would give us a particle flux directed outwards. At the same time the mode with maximum γ is pretty much in the middle between the outward and inward branches, and in this particular case it agrees with the non-linear result.

In spite of an agreement between linear GS2 and non-linear GYRO for this plasma conditions, there is no guarantee that they produce similar results for all plasma parameters considered in this paper. Performing non-linear simulations like the one presented on Fig. 10 for the full range of parameter would be extremely expensive in terms of computer time and currently unrealistic. However a more complete study of density peaking on collisionality and other parameters in non-linear gyrokinetics is planned for the future [13]

CONCLUSIONS.

On the basis of JET H-mode experiments we were able to find empirical relations which describe density peaking as a function of ν_{eff}, T_i/T_e, particle sources (Γ') and l_i. The general conclusions remained the same as in previous publications based on earlier experiments on the JET and AUG tokamaks: the effective collisionality plays a crucial role in plasma density gradient formation, extrapolation of the current experimental observations to ITER specific plasma parameters predicts moderately peaked density profile for the baseline H-mode scenario.

Using the GS2 code we performed numerous simulations varying the parameters involved in empirical scaling relations. The results of quasilinear analysis based on the max. γ mode are in a good agreement with the experiments. Non-linear collisional GYRO simulation partially supports the linear simulations but still requires a deeper study.

AKNOWLEDGEMENTS

The authors thank W. Dorland and M. Kotschenreuther for providing the gyrokinetic code GS2, as well J. Candy and R.E. Waltz for providing the GYRO code. This work was supported in part by the Swiss National Science Foundation. This work, supported by the European Communities under the contract of Association between EURATOM/CRPP, was carried out within the framework of the European Fusion Development Agreement. The views and opinions expressed herein do not necessarily reflect those of the European Commission.

REFERENCES

[1]. Angioni C. et al. Nucl. Fusion **47** (2007) 1326-1335
[2]. Weisen H. et al. 2006 Plasma Phys. Control. Fusion **48** A457-66
[3]. Weisen H. et al, Nucl. Fusion **45** (2005) L1-L4
[4]. Angioni C., Peeters A.G. et al, Phys. Rev. Lett. 90, 205002 (2003)
[5]. M. Greenwald, Angioni C. et al, Nucl. Fusion **47** (2007) L26-L29
[6]. Challis C.D. et al, Nuclear Fusion, **29** (1989) 563
[7]. Stix T.H., Plasma Physics, vol **14**, (1972) 367-384
[8]. Mukhovatov V., Shimomura Y., Polevoi A. et al, Nucl. Fusion **43** (2003) 942-948
[9]. Kotschenreuther M., Rewoldt G. and Tang W.M., Comput. Phys. Commun. **88**, 128 (1995)
[10]. Dorland W. et al, Phys. Rev. Lett. vol. 85, num 28 (200)
[11]. Angioni C. et al, Physics of Plasmas **12**, 112310 (2005)
[12]. Jenko F., Dannert T., Angioni C., Plasma Phys. Control. Fusion **47** (2005) B195-B206
[13]. Angioni C., to be published

	$n_{02}/\langle n\rangle$	R/L_n	$\nu_{eff}^{1/2}$	Γ'	ρ^*	T_i/T_e	q_{95}	β_N	R/L_{Te}	R/L_{Ti}	l_i	δ
$n_{02}/\langle n\rangle$	**1**	**0.92**	**-0.71**	0.53	-0.13	0.4	-0.05	-0.36	-0.22	0.09	0.31	-0.52
R/L_n	**0.92**	**1**	**-0.67**	0.54	0.02	0.41	-0.15	-0.19	-0.08	0.08	0.3	-0.43
$\nu_{eff}^{1/2}$	**-0.71**	**-0.67**	**1**	-0.42	0.25	-0.23	0.13	0.5	0.25	-0.04	-0.27	**0.69**
Γ'	0.53	0.54	-0.42	**1**	0.24	**0.93**	0.05	0.06	-0.01	-0.22	-0.13	-0.16
ρ^*	-0.13	0.02	0.25	0.24	**1**	0.4	-0.41	**0.88**	0.48	-0.28	-0.52	0.58
T_i/T_e	0.4	0.41	-0.23	**0.93**	0.4	**1**	0.04	0.18	0.1	-0.19	-0.27	-0.03
Q_{95}	-0.05	-0.15	0.13	0.05	-0.41	0.04	**1**	-0.21	-0.32	-0.2	-0.06	-0.06
β_N	-0.36	-0.19	0.5	0.06	**0.88**	0.18	-0.21	**1**	0.44	-0.42	-0.48	**0.78**
R/L_{Te}	-0.22	-0.08	0.25	-0.01	0.48	0.1	-0.32	0.44	**1**	0.23	-0.01	0.37
R/L_{Ti}	0.09	0.08	-0.04	-0.22	-0.28	-0.19	-0.2	-0.42	0.23	**1**	0.54	-0.28
l_i	0.31	0.3	-0.27	-0.13	-0.52	-0.27	-0.06	-0.48	-0.01	0.54	**1**	-0.45
δ	-0.52	-0.43	**0.69**	-0.16	0.58	-0.03	-0.06	**0.78**	0.37	-0.28	-0.45	**1**

Table 1: Cross correlation coefficients between various experimental parameters (v_{eff}<0.5)

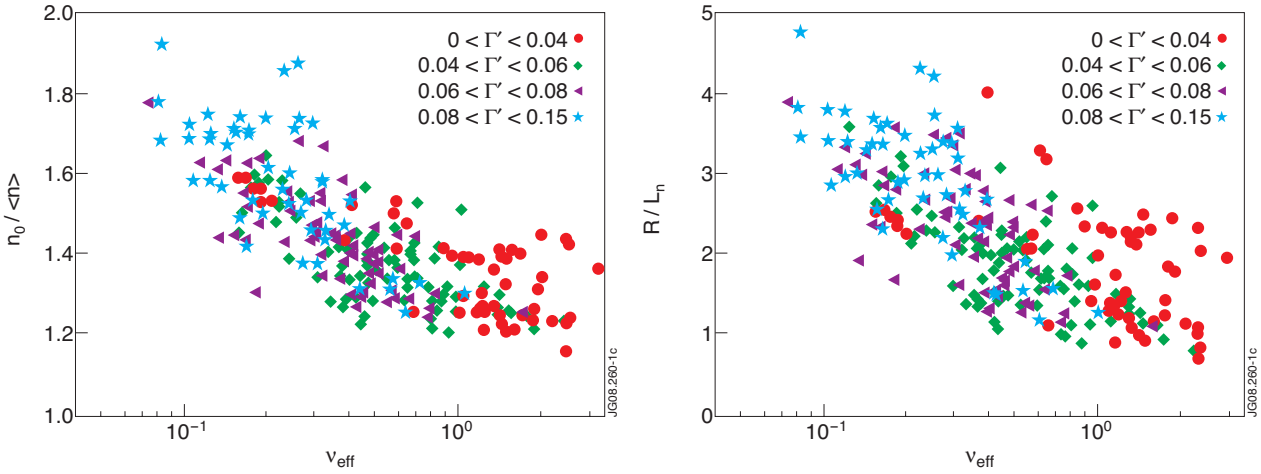

Figure 1: Density peaking (left) and normalized density gradient (right) as a function of the effective collisionality.

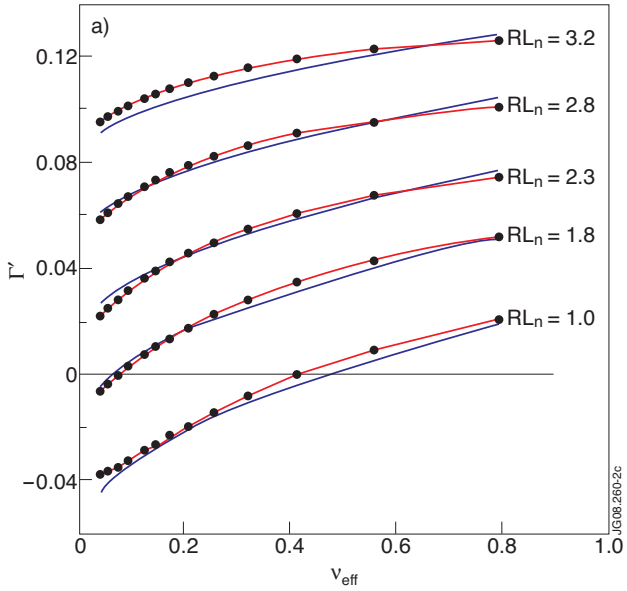

Figure 2: GS2 simulation results for T_i/T_e=1, R/L_{Ti}=R/L_{Te}=6.0. Blue thin line – approximation of Γ_{GS2} with formula (4)

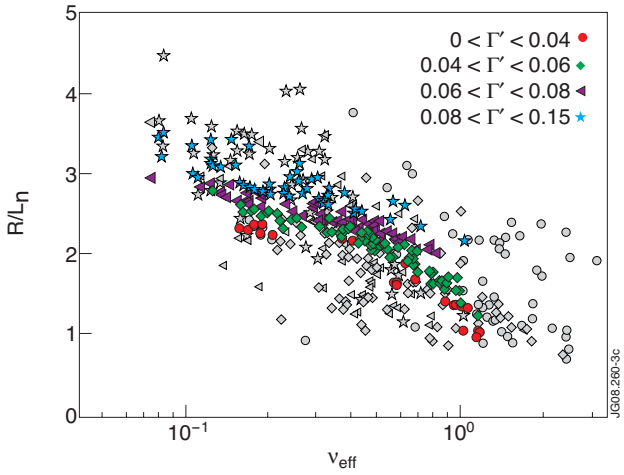

Figure 4: expected R/L_n values in JET database for R/L_{Ti}=7.0, 8.0, 9.0 with respect to initial R/L_{Ti}=6.0 case.

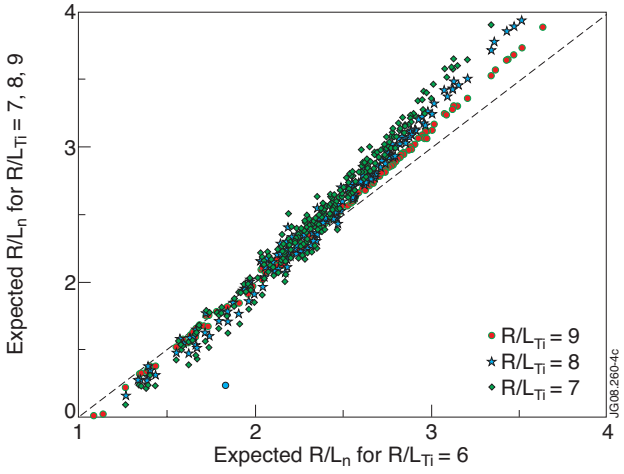

Figure 3: Comparison of simulation (colored points) with experimental results (grey points). Different symbols correspond to different Γ

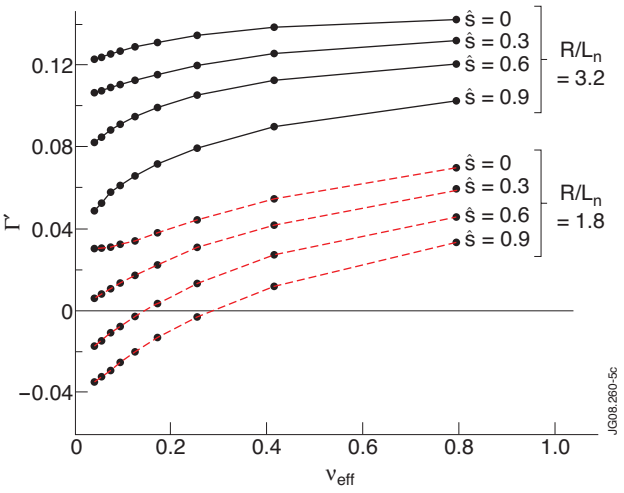

Figure 5: Γ from GS2 simulations with different R/L_n and $\hat{s}$ inputs. T_i/T_e=1, R/L_{Ti}=R/L_{Te}=6.0

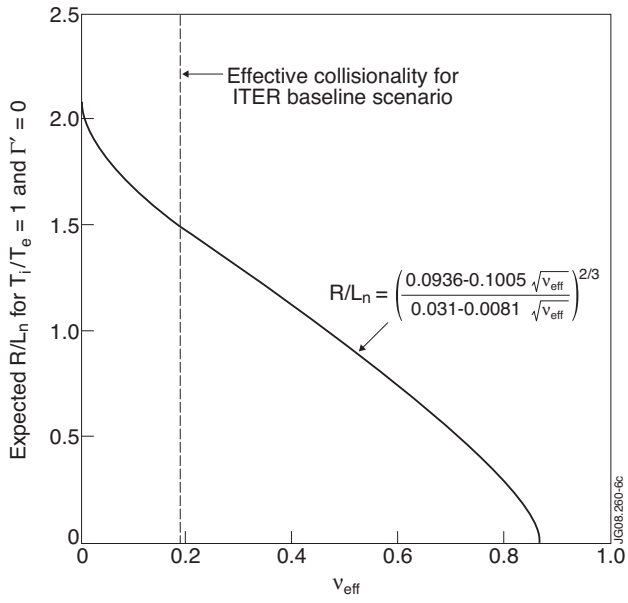

Figure 6: R/L_n estimation for Γ=0 and T_i=T_e

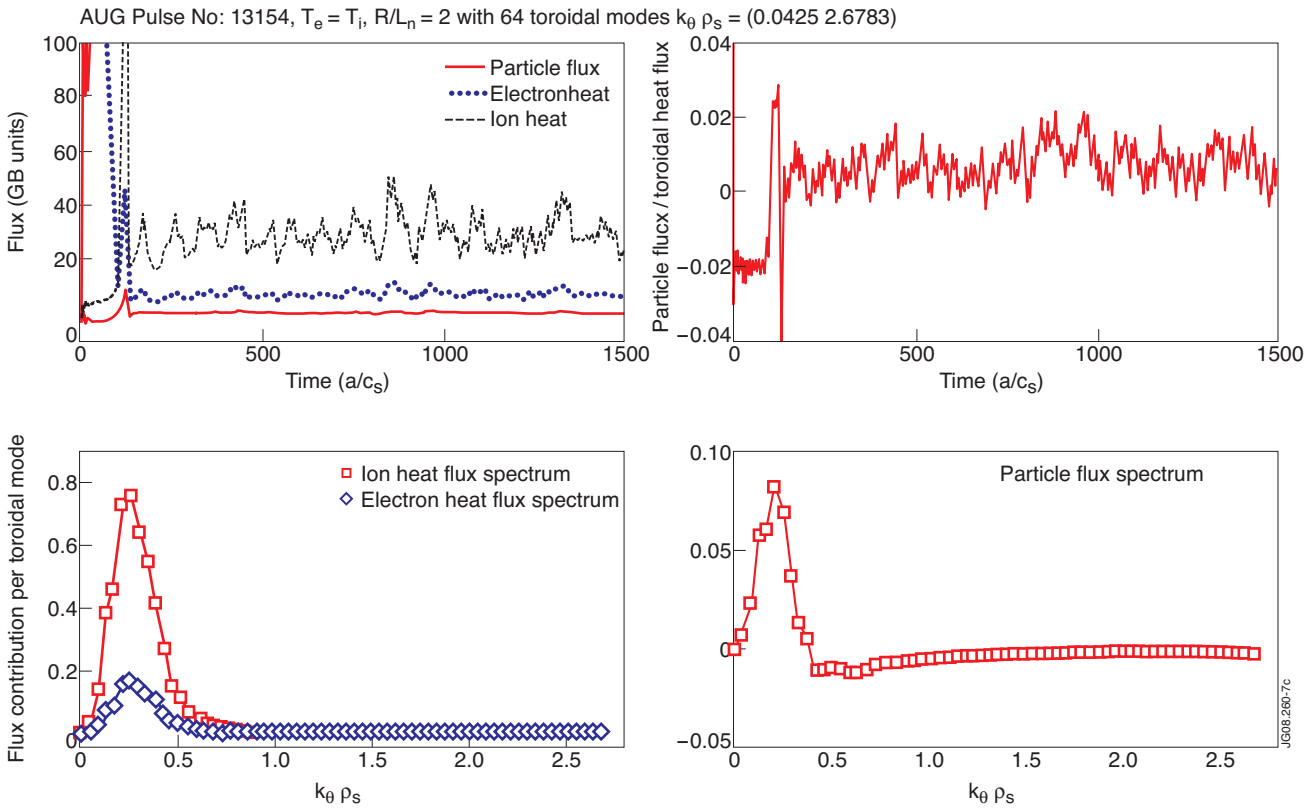

Figure 7: Non-linear GYRO simulation result top-left: heat and particle fluxes versus time. top-right: particle over heat flux versus time bottom-left: k_y spectrum for the heat flux bottom-right: k_y spectrum for the part. flux